Dijet photoproduction of massless charm jets
at next-to-leading order of QCD

Michael Klasen[a][*] and Gustav Kramer[b]

[a] *Institut für Theoretische Physik, Westfälische Wilhelms-Universität Münster,*

Wilhelm-Klemm-Straße 9, D-48149 Münster, Germany

[b] *II. Institut für Theoretische Physik, Universität Hamburg,*

Luruper Chaussee 149, D-22761 Hamburg, Germany

(Dated: April 4, 2011)

Abstract

We compute the charm dijet photoproduction cross section at next-to-leading order of QCD in the zero-mass variable flavour number scheme, i.e. with active charm quarks in the proton and photon. The results are compared to recent measurements from the ZEUS experiment at HERA. The predictions for various distributions agree well with the data, in particular for large momentum fractions of the the partons in the photon, where direct photon processes dominate. At low momentum fractions, the predictions are quite sensitive to the charm content in the photon. The experimental data are shown to favour parameterizations with a substantial charm quark density such as the one proposed by Cornet et al.

---

[*]klasen@lpsc.in2p3.fr

I. INTRODUCTION

In photoproduction processes at HERA, a quasi-real photon emitted from the incoming electron (or positron) collides with a parton from the incoming proton. Within QCD the photoproduction is classified into two categories: (i) direct processes, in which the photon acts as a point-like particle in the hard scattering, and (ii) resolved processes, in which the photon acts as a source of incoming partons which participate in the hard interaction. The two classes result directly from the next-to-leading order (NLO) QCD calculation of the photoproduction cross sections, since due to the initial photon's virtuality $Q^2 = 0$, the direct processes in NLO have an initial-state singularity which must be absorbed into the photon parton distribution functions (PDFs), on which the resolved cross section depends.

Measurements of cross sections for the production of jets with high transverse energy are sensitive to the PDFs of both the proton and the photon. The proton PDFs are known from the extensive global analyses of the CTEQ [1] and MSTW [2] groups. The photon PDFs are essentially based only on data for $F_2^\gamma(x)$. Of course the proton PDFs are much better known than the photon PDFs. The three newest photon PDFs, Cornet et al. (CJK) [3], Aurenche et al. (AFG04) [4] and Slominski et al. (SAL) [5], use all available data of F_2^γ from the LEP experiments. The older parameterizations of Glück et al. (GRV) [6] and Aurenche et al. (AFG) [7] could use only the lower energy measurements of F_2^γ known at the time of their construction and are, of course, less reliable than the more recent sets.

In 2007 the ZEUS collaboration at HERA presented their data on high-E_T dijet photoproduction [8] and compared them to NLO QCD calculations with the aim to provide constraints on the PDFs of the photon. The comparison was done to the five photon PDFs mentioned above. The differences obtained with these PDFs were generally less than 25% for the AFG, AFG04, SAL and GRV sets. The predictions based on CJK set was up to 70% higher than those based on the other four. These differences occurred predominantly in the small x_γ region and for low E_T. Otherwise the agreement with all five PDFs was very satisfactory. The photon PDFs have three essentially different components: light quarks, heavy quarks (charm and/or bottom) and the gluon. The best known of these three components is that of the light quarks, while much less is known about the charm and bottom quark contents. However, it is possible to separate the heavy quarks, for example the charm quark PDF in the photon, from the light quark ones by measuring the dijet production

cross sections with at least one charm quark jet. Such measurements have been done in the past by the ZEUS collaboration at HERA [9–11]. In these measurements the selection of the charm jet occurs by measuring the differential cross section for the production of a D^*-meson associated with the dijet system. So far, these data have been compared only with NLO predictions based on the massive charm scheme or fixed-flavour number scheme (FFNS) [12], in which an explicit charm component of the photon PDFs in the resolved cross section does not occur. In this scheme such a contribution is approximated with the NLO partonic cross section, convolved with the PDFs of incoming light quarks and the gluon. On the other hand in the comparison of the inclusive dijet photoproduction data (see for example [8] and the earlier work quoted there) with the NLO calculations, the charm quark is always considered massless with the consequence that in the resolved contribution the charm component of the photon PDFs is present. This approach would be justified when the cross section with at least one charm could satisfactorily be described in the massless charm scheme.

It is the purpose of this work to present results of NLO calculations in the massless charm scheme for dijet cross sections with at least one charm jet and to find out whether they can describe satisfactorily the measured cross sections from ZEUS [10]. There, a similar comparison had been performed, which was, however, based only on leading order Monte Carlo simulations. Of course such a comparison depends on the charm PDF of the photon. The treatment of the charm quark being massless is justified as long as the E_T of the produced jets is large enough, i.e. $E_T^2 \gg m^2$, where m is the charm quark mass. The ZEUS data reported in [10] are particularly suitable for our purpose, since by measuring the x_γ distribution $d\sigma/dx_\gamma$ and the angular distribution of the outgoing jets for large and small x_γ, i.e. for the dominant subprocesses, direct and resolved, the data are most sensitively dependent on the charm content of the photon PDF.

In section 2 we shall describe the theoretical framework and outline the kinematical restrictions based on the experimental cuts applied in [10]. Section 3 contains our results and the discussion of the comparison with the data [10] for the default choice of the GRV photon PDF. In section 4 we compare different photon PDFs for a scale characteristic for charm jet production, and in section 5 we give cross sections obtained with three different photon PDFs, GRV, AFG04 and CJK. Our conclusions are presented in section 6.

II. THEORETICAL FRAMEWORK AND KINEMATICAL CONSTRAINTS

For our calculations we rely on our work on dijet production in the reaction $\gamma + p \rightarrow jets + X$ [13] in which we have calculated the cross section for inclusive one-jet and two-jet production up to NLO for both the direct and the resolved contribution (for a review see [14]). The predictions of this work have been tested by many experimental studies of the H1 and ZEUS collaborations at HERA. To obtain the cross section with at least one charm jet in the final state we calculated the difference of the cross section with $n_f = 4$ quark flavours and the cross section with $n_f = 3$ quark flavours in the initial state. In the resolved part this difference contains only the contribution of $cg, \bar{c}g, cq, \bar{c}q$ and $c\bar{c}$ in the initial state, where q is a light quark (or antiquark). In the $c\bar{c}$ contribution it contains also the contribution from $c\bar{c} \rightarrow gg$ and $c\bar{c} \rightarrow q\bar{q}$ in leading order (LO) and the corresponding contributions in NLO. Since these contributions originate from the charm PDFs of the photon and the proton, their magnitude is expected to be small. In LO their contribution to the cross section integrated over the whole phase region as in the ZEUS experiment, to be specified below, amounts to 0.3%. We expect a similar amount from the NLO contributions. As input we employ the NLO GRV 92 photon PDFs [6], converted to the $\overline{MS}$ scheme, and the NLO CTEQ6M proton PDFs [15]. The strong-coupling constant $\alpha_s^{(n_f)}(\mu_R)$ is evaluated from the two-loop formula [16] with n_f active quark flavours. Both in the $n_f = 3$ calculation and in the difference of the $n_f = 4$ and $n_f = 3$ cross sections, $n_f = 4$ is used in the α_s formula. The asymptotic scale parameter is $\Lambda_{\overline{MS}}^{(4)} = 0.347$ GeV corresponding to $\alpha_s^{(5)}(m_Z) = 0.118$. We choose the renormalization scale μ_R and the factorization scale μ_F of the initial state to be $\mu_R = \xi_R \bar{E}_T$ and $\mu_F = \xi_F \bar{E}_T$, where $\bar{E}_T$ is the average transverse energy of the two (or three)final-state partons constituting the two jets. ξ_R and ξ_F are dimensionless scale factors, which are varied about their default values $\xi_R = \xi_F = 1$ as described later. The experimental data presented in [10] were taken with electrons or positrons of energy $E_e = 27.5$ GeV and protons with energy $E_p = 820$ GeV (1996-1997) or $E_p = 920$ GeV (1998-2000) corresponding to integrated luminosities of 38.6 ± 0.6 and 81.9 ± 1.8 pb^{-1} and to centre-of mass energies of $\sqrt{s} = 300$ GeV and $\sqrt{s} = 318$ GeV, respectively. In our calculations we took the kinematic conditions of the 1998-2000 period due to its larger luminosity.

In the experiment, the photon virtuality Q^2 was restricted to be below $Q_{max}^2 = 1 \; GeV^2$. The photon-proton centre-of mass energy was lying in the range $130 < W < 280$ GeV. Jets

were reconstructed with the k_T-cluster algorithm in the longitudinally invariant inclusive mode [17]. The events were required to have at least two jets with pseudorapidity $|\eta^{jet}| < 2.4$ and transverse energy $E_T > 5.0$ GeV. With the two energetic jets a D^*-meson is observed. The reconstructed D^* meson is required to have $p_T^{D^*} > 3$ GeV and pseudorapitity $|\eta^{D^*}| < 1.5$.

In [10], the following three jet variables were chosen in the analysis: x_γ^{obs}, x_p^{obs} and $\cos\Theta^*$. In order to select contributions to the cross section enriched by direct and resolved photon events, the variable x_γ^{obs} defined by

$$x_\gamma^{obs} = \frac{\sum_{jets}(E_T^{jet} e^{-\eta^{jet}})}{2yE_e} \tag{1}$$

was determined. Here, yE_e is the initial photon energy, and the sum in Eq. (1) is over the two jets with the two highest E_T^{jet}. Due to the restriction to two jets, x_γ^{obs} does not measure the full x_γ, whence the superscript "obs". With $x_\gamma^{obs} > (<)0.75$ samples enriched in direct (resolved) photon processes are selected. The complementary variable on the proton side is

$$x_p^{obs} = \frac{\sum_{jets}(E_T^{jet} e^{\eta^{jet}})}{2E_p}, \tag{2}$$

which is the fraction of the proton's momentum contributing to the production of the two jets with highest E_T^{jet}. The third variable is $\cos\Theta^*$, where Θ^* is the dijet scattering angle. It is given by

$$\cos\Theta^* = \tanh((\eta^{jet1} - \eta^{jet2})/2). \tag{3}$$

In order to enhance the characteristic features of the direct versus the resolved contributions in the $\cos\Theta^*$ distribution, a cut on the invariant mass M_{jj} is applied: $M_{jj} > 18$ GeV. For the case in which the two jets are back-to-back in the transverse plane with equal transverse E_T, the dijet invariant mass is

$$M_{jj} = \frac{2E_T^{jet}}{\sqrt{1 - |\cos\Theta^*|^2}}. \tag{4}$$

In order to achieve high values of $|\cos\Theta^*|$ without bias from the E_T^{jet} cut, M_{jj} must be large enough. In our calculations we shall study only the distribution in the absolute value of $\cos\Theta^*$, which does not depend on which is jet number 1 and jet number 2. In the data analysis of [10] a cut on the average longitudinal boost $\bar{\eta} = (\eta^{jet1} + \eta^{jet2})/2$ of $\bar{\eta} < 0.7$ is applied. This selection limits η^{jet} to $|\eta^{jet}| < 1.9$, removes the bias caused by the explicit cut on η^{jet} and reduces the bias caused by the cut on $|\eta^{D^*}| < 1.5$. According to [10] the

residual distortion due to η^{D^*} cut is small and confined to the extreme bins of the $\cos \Theta^*$ distribution. With all these cuts it is achieved that the measured distributions test to a large extent the dynamics of the hard scattering processes.

All these experimented cuts on the rapidities η^{jet}, transverse energies E_T^{jet} and the invariant mass M_{jj} are also applied to the calculation of the cross sections in NLO. However, the $E_T^{jet} \geq 5.0$ GeV cut to both jets cannot be applied, since it leads to infrared sensitive cross sections [18]. Therefore we choose $E_T^{jet1} \geq 5.5$ GeV and $E_T^{jet2} \geq 5.0$ GeV. Unfortunately, in the experimental data analysis such an asymmetric cut has not been applied, although in an earlier [9] and the later publication [11] such asymmetric cuts were used to make the comparison with the results of the massive NLO calculations possible. Since with our choice the difference between the two cut values is small, 0.5 GeV, we expect that it has little influence on the measured cross sections.

The observed D^* in every event triggers the production of at least one charm jet. The fraction of charm quarks fragmenting into a D^* meson was assumed to be 0.235 [19]. We multiply the calculated charm jet cross section with this branching ratio when we compare to the experimental data. Actually the measured cross sections are the luminosity-weighted average of the cross sections at the two proton energies $E_p = 820$ GeV and $E_p = 920$ GeV. In our calculation we neglect this averaging and give only results for $E_p = 920$ GeV.

III. RESULTS FOR GRV PHOTON PDFS AND COMPARISON WITH ZEUS DATA

In connection with inclusive dijet events obtained for our calculation with $n_f = 4$ initial quark flavours, it is of interest to know the contributions of charm dijet events. Therefore, we have calculated the ratio of the charm jet dijet cross section to the inclusive dijet cross section. This ratio is shown as a function of x_p^{obs} (denoted as x_p in the figure) in Fig. 1. The ratio is of order 30% and almost independent of x_p. If the direct process dominated, this ratio would be 2/5 as follows from the sum of the squared charges of the contributing quarks. The smaller ratio in Fig. 1 is due to the contribution of the resolved process.

The differential charm dijet cross section as a function of x_γ^{obs} (denoted x_γ in the figure), which is sensitively dependent on the resolved process for $x_\gamma^{obs} < 1$, is plotted in Fig. 2 and compared with the data from [10]. To the theoretical NLO predictions we have applied
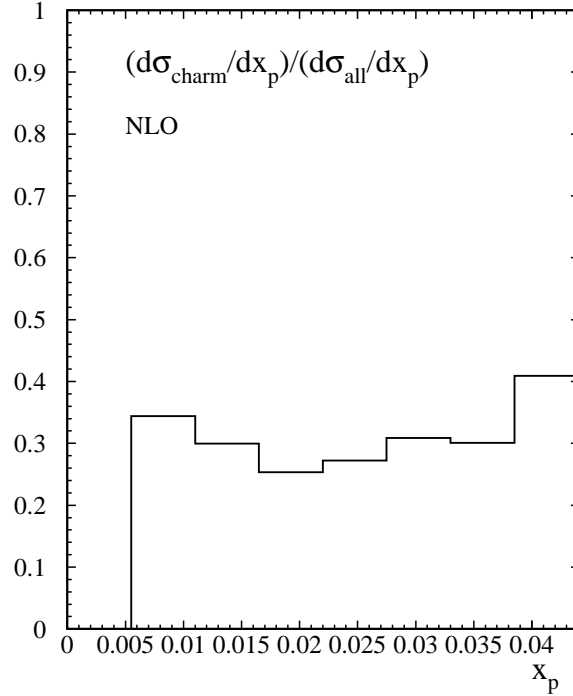
6

FIG. 1: Ratio of the charm dijet cross section $d\sigma/dx_p$ to the full dijet cross section (all flavours up to charm) as a function of x_p.

hadronization corrections, which have been given in [20]. In each bin the NLO cross section was multiplied by the correction factor $C_{had} = \sigma_{MC}^{hadron}/\sigma_{MC}^{parton}$, which is the ratio of the Monte Carlo (MC) cross sections after and before the hadronization process. In addition, we have evaluated the uncertainties in the NLO calculations, shown as the shaded area, originating from the variation of μ_R and μ_F with the parameters ξ_R and ξ_F in the range $0.5 \leq \xi_R, \xi_F \leq 2.0$ and $0.5 \leq \xi_R/\xi_F \leq 2.0$. The maximum (minimum) cross section is obtained for $\xi_R = 1.0$, $\xi_F = 2.0$ ($\xi_R = 1.0$, $\xi_F = 0.5$). This variation of scales is also used in connection with the x_p^{obs} and $|\cos\Theta^*|$ distributions shown below. The low-x_γ tail of the NLO cross section is below the data. For $x_\gamma^{obs} > 0.75$, the data are well described by the NLO prediction. In the region $x_\gamma^{obs} < 0.75$ we would have expected a better agreement with the data since in this region the higher order terms to the cross section contribute together with the resolved contribution. However, the NLO direct terms give a negative contribution in this region which apparently is not compensated enough by the resolved contribution. From this comparison we can conclude already that the charm part of the photon PDF as
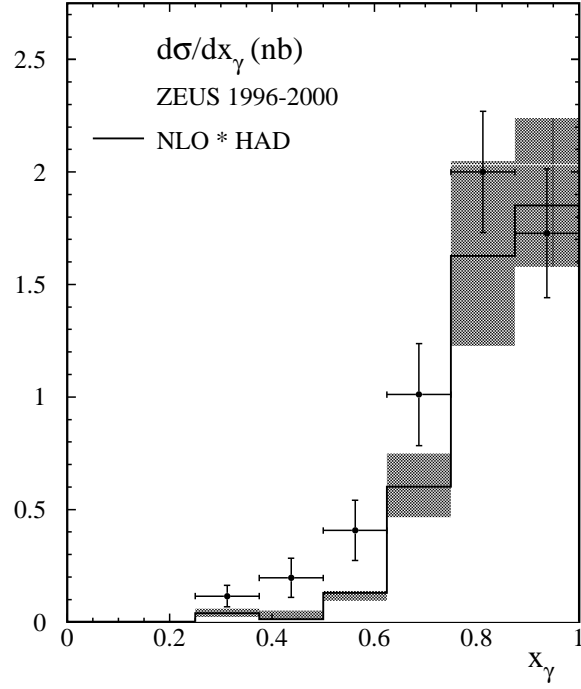
7

FIG. 2: Differential cross section $d\sigma/dx_\gamma$ as a function of x_γ compared to the data of [10].
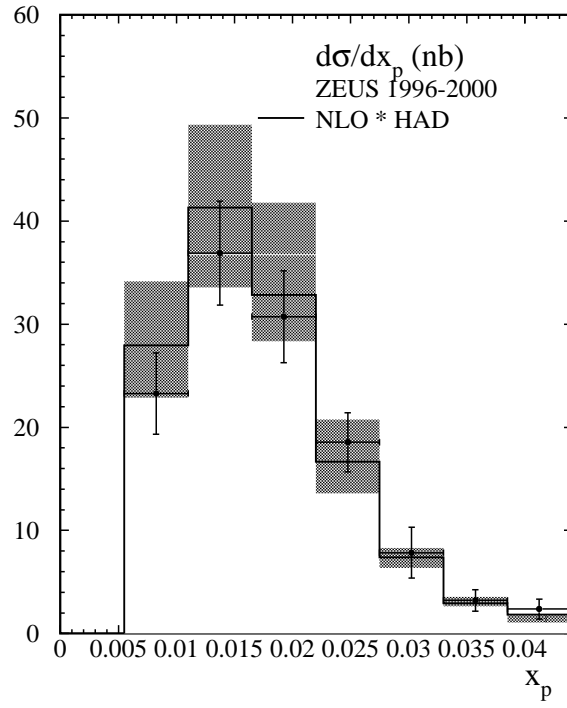

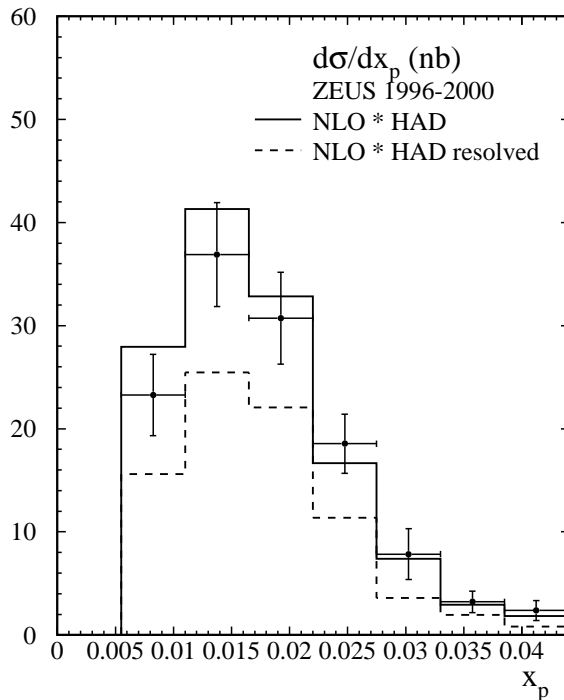FIG. 3: Differential cross section $d\sigma/dx_p$ as a function of x_p compared to data of [10].

FIG. 4: Resolved part of the differential cross section $d\sigma/dx_p$ as a function of x_p compared to the full cross section and to data of [10].

contained in the GRV higher order set [6] is not large enough in the low x_γ region. We shall come back to this point when we discuss other parameterizations of the charm PDFs of the photon.

The differential cross section as a function of x_p^{obs} is compared in Fig. 3 with our NLO calculation. The NLO prediction is in good agreement with the data. All data points lie inside the theoretical error range, even the point in the largest x_p^{obs} bin agrees inside the experimental error. Actually for the default scales $\xi_R = \xi_F = 1.0$ the theoretical prediction agree with the data inside the experimental error. It is of interest to know how much of the cross section $d\sigma/dx_p^{obs}$ originates from the direct or resolved part of the cross section. This is shown in Fig. 4, where we have plotted the resolved part of $d\sigma/dx_p$ and compared with the full $d\sigma/dx_p$ and the experimental data of [10]. We see that the resolved part has almost the same shape and its strength is between 50 and 60% of the total. The direct-*enriched* x_p distribution, i.e. for $0.75 \leq x_\gamma \leq 1.0$, is between 80 and 95%, depending on x_p. Thus the resolved-*enriched* contribution of $d\sigma/dx_p$, i.e. for $0 \leq x_\gamma \leq 0.75$, is very small. Due to the
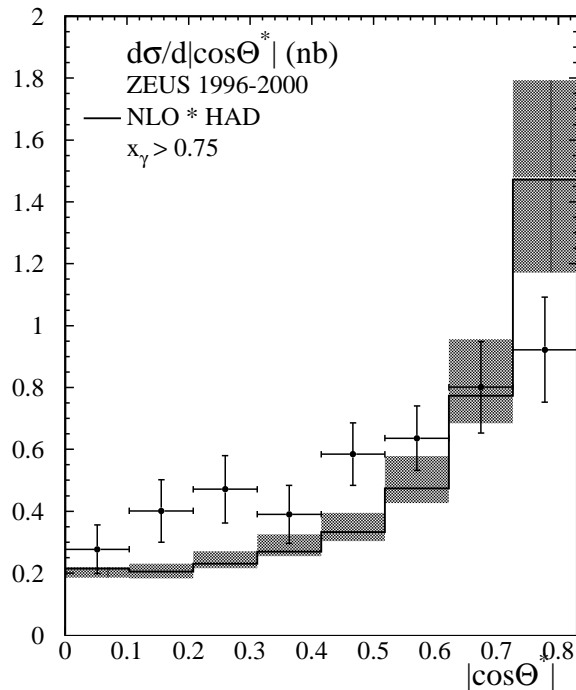
FIG. 5: Differential cross section $d\sigma/d|\cos\Theta^*|$ as a function of $|\cos\Theta^*|$ for $x_\gamma > 0.75$ compared to the data of [10].

lack of data for it in [10], a direct comparison is not possible.

In Fig. 5 and Fig. 6 we compare the NLO results for the charm dijet angular distribution to the ZEUS data [10] as a function of $|\cos\Theta^*|$. For the high-x_γ region, $0.75 < x_\gamma < 1.0$ (see Fig. 5), the NLO result is in reasonable agreement with the data, although not perfect even inside the theoretical error bars, which are rather small for the lower $|\cos\Theta^*|$ bins. For low x_γ, $0 < x_\gamma < 0.75$ (see Fig. 6), the NLO prediction is much lower than the data, except for the two lowest $|\cos\Theta^*|$ bins. This is related to the bad agreement between the prediction and the data for the $d\sigma/dx_\gamma$ cross section in the region $x_\gamma < 0.75$, where apparently contributions from the resolved part are missing. Actually the experimental data agree much better with the LO prediction using the same PDFs for the proton and the photon as in the NLO calculation. The LO cross section for $d\sigma/d|\cos\Theta^*|$ is, depending on the $|\cos\Theta^*|$ bin, up to a factor between 1.1 and 2.7 larger than the NLO result.

In total we can state that our results with the GRV photon PDFs [6] agree reasonably well with the data of [10] in the large-x_γ region, but much less so in the small-x_γ region, where
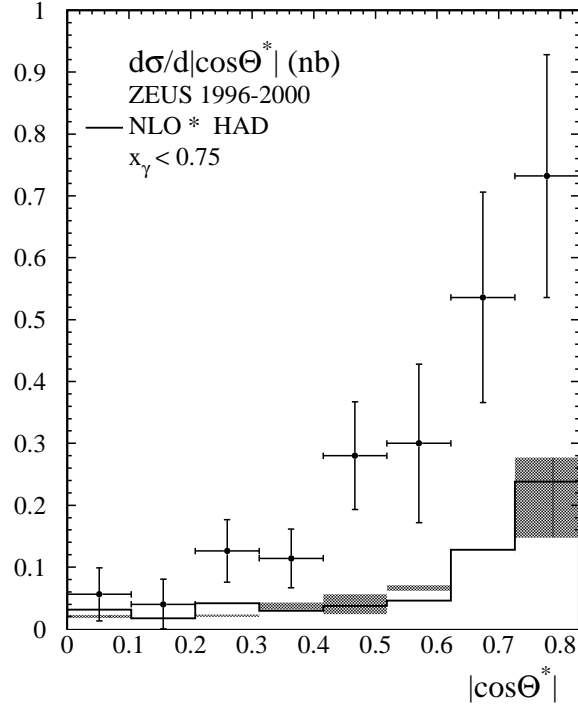
10

FIG. 6: Differential cross section $d\sigma/d|\cos\Theta^*|$ as a function of $|\cos\Theta^*|$ for $x_\gamma < 0.75$ compared to the data of [10].

the calculated cross sections are too small as compared to the experimental cross sections of [10]. This is quite similar as the results obtained in [10] in the FFN scheme. From this comparison we conclude that replacing the massless charm cross section in the calculations for the inclusive dijet photoproduction cross section by the FFNS result would not change the result significantly. In the FFNS calculations the resolved contribution depends only on the photon PDFs of the light quarks and the gluon. Therefore, we do not expect that the FFNS result will change much by choosing other photon PDFs, also in particular since in the FFN scheme the resolved contribution is less than in the massless charm scheme. Therefore, a change of the theoretical result in the small-x_γ region can be achieved only in the massless charm scheme by changing in the resolved contribution the charm part of the photon PDFs. To see whether this is possible we shall investigate in the follwing the theoretical cross sections in the small-x_γ region with the more modern photon PDFs AFG04 [4] and CJK [3] with the hope that the cross section in this region will be larger.
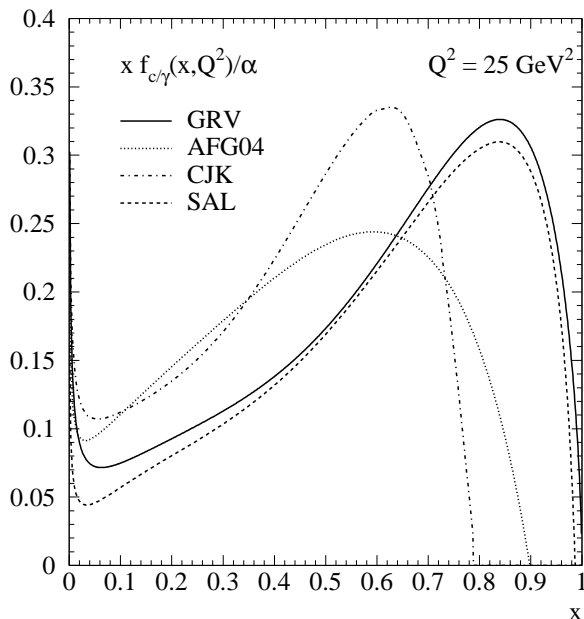
FIG. 7: Charm densities in the photon.

IV. CHARM DENSITIES IN THE PHOTON

Before we present our results, we shall take a look at the differences between the charm densities of the various photon PDFs as a function of the scaled momentum variable x for the scale $Q^2 = 25 \ GeV^2$, which is the smallest squared scale occurring in our cross section calculations. The four charm desities of the photon are plotted in Fig. 7 as a function of x in the interval $0 \leq x \leq 1$. To make the comparison easier, the photon PDFs are shown in the DIS_γ scheme in order to regularize the singularity at $x \to 1$. Shown is the GRV charm density [6], which is already given in the DIS_γ scheme. An updated version of this is the PDF GRS [21], but this does not include a charm density. This is explicitly described by the LO FFNS contribution in F_2^γ, which is not suitable for our purpose. The next one is AFG04 [4], which is constructed in the $\overline{MS}$ scheme and therefore transformed to the DIS_γ scheme by adding the term C_γ [4]. For this density $m_c = 1.41$ GeV, so at $Q^2 = 25$ GeV^2, $x_{\rm th} = Q^2/(Q^2 + 4m_c^2) = 0.76$. But this is not reflected in the charm PDF, since it is constructed in the massless flavour changing scheme with $n_f = 5$. This charm density changes very little as compared to the older version AFG [7]. It is considerably larger (smaller) than the GRV version at $x < 0.65$ ($x > 0.65$). The CJK charm
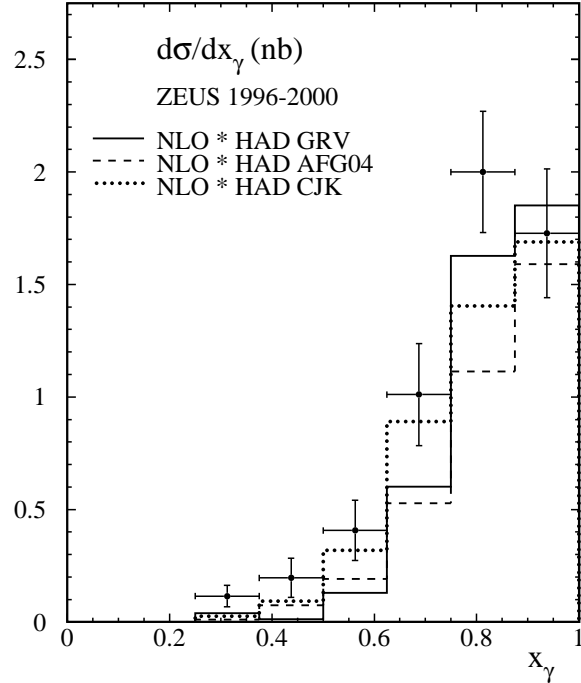
FIG. 8: Differential cross sections $d\sigma/dx_\gamma$ for GRV, AFG04 and CJK photon PDFs compared to data of [10].

density is alo presented in the DIS_γ scheme [3]. Here $m_c = 1.3$ GeV, so at $Q^2 = 25$ GeV^2, $x_{\rm th} = Q^2/(Q^2 + 4m_c^2) = 0.79$. This is clearly visible in the charm PDF, since the finite charm mass is kept. It is considerably larger (smaller) than GRV at $x < 0.7$ ($x > 0.7$). The SAL charm density is also obtained in the DIS_γ scheme [5]. Here $m_c = 1.5$ GeV is used, but it enters only at threshold in the α_s evolution. It is very similar to GRV, but it is slightly lower over the full range of x, in particular at small $x \leq 0.05$. Because of the similarity to our default choice GRV, we do not expect important changes in the dijet cross sections and therefore do not consider it further.

From this comparison, we expect that the AFG04 and even more so the CJK charm photon PDFs should yield larger cross sections than the GRV version in the small-x_γ^{obs} region and somewhat smaller coss sections in the large-x_γ^{obs} region. How the cross sections for these three photon PDFs, GRV, AFG04 and CJK, compare with each other and with the ZEUS data will be shown in the next section.
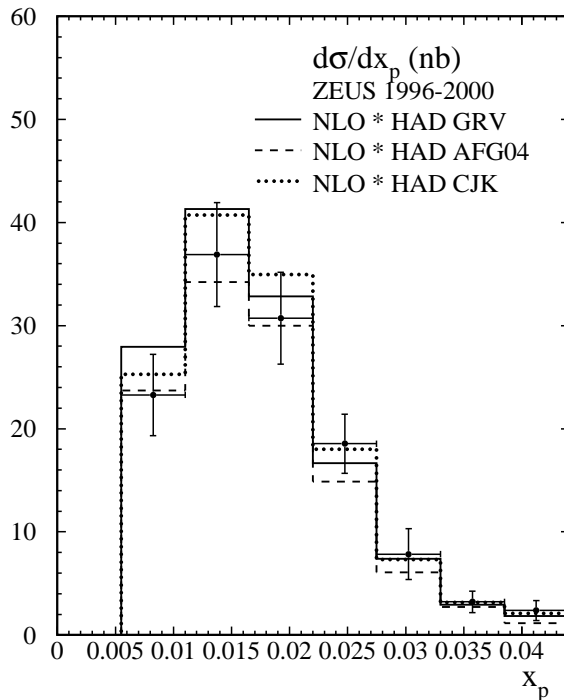
13

FIG. 9: Differential cross section $d\sigma/dx_p$ for GRV, AFG04 and CJK photon PDFs compared to data of [10].

V. RESULTS FOR GRV, AFG04 AND CJK PHOTON PDFS

First we show the cross section $d\sigma/dx_\gamma$ in Fig. 8 for the three photon PDFs GRV, AFG04 and CJK, where we expect better agreement with the experimental cross section for $x_\gamma < 0.75$ with CJK. This is indeed the case. Whereas in the two largest x_γ-bins there is little change between GRV and CJK, the rest of the x_γ-bins have larger cross sections for CJK and agree now much better with the ZEUS data. For completeness we also show the equivalent comparison for the cross section $d\sigma/dx_p$ (Fig. 9). Here all three photon PDFs yield almost the same cross section and agree equally well with the data. A similar pattern occurs for the $|\cos\Theta^*|$ distribution in the large x_γ region ($x_\gamma > 0.75$). The cross section for the three PDFs are very similar and agree equally with the ZEUS data. Only at $|\cos\Theta^*| \sim 0.8$ the cross setion for AFG04 and CJK is somewhat reduced (see Fig. 10). The critical cross section is $d\sigma/d|\cos\Theta^*|$ for $x_\gamma < 0.75$ shown in Fig. 11. Here the agreement with the data was bad for GRV, in particular for $|\cos\Theta^*| > 0.3$. In this region the data agree now better with the CJK prediction as expected, although not perfectly. The cross
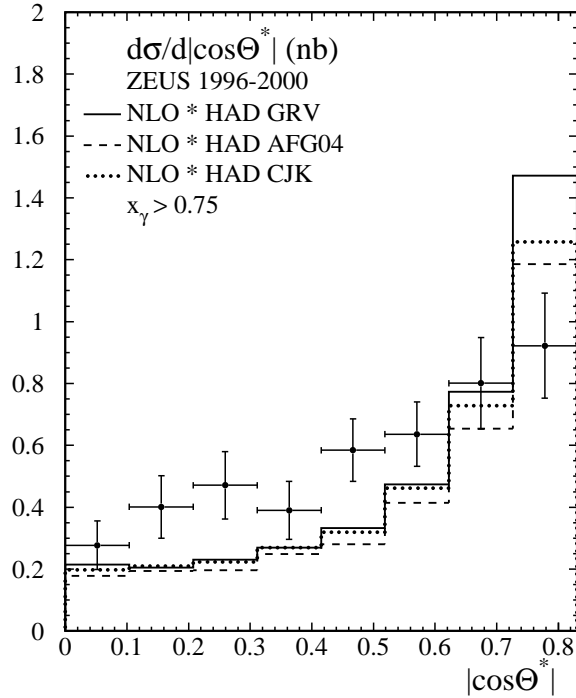
14

FIG. 10: Differential cross section $d\sigma/d|\cos\Theta^*|$ with the constraint $x_\gamma > 0.75$ for GRV, AFG04 and CJK photon PDFs compared to data of [10].

section for CJK is more than a factor of two larger than for GRV in this region of $|\cos\Theta^*|$. The result for AFG04 is very similar to that of GRV and does not lead to any improvement compared to the experimental results.

As mentioned in the introduction, the dijet photoproduction cross section as a function of x_γ has been measured by the ZEUS collaboration also for all flavours [8], and the comparison with NLO calculations showed in general good agreement for all tested photon PDFs. However, the NLO predictions obtained with the CJK photon PDFs were larger than the data at low $x_\gamma \leq 0.6$ and $E_T \simeq 20$ GeV, while they agreed better with the data than those obtained with the other PDFs in the second and larger E_T-bins. It may thus be necessary to compensate the higher charm-quark density favoured by the charm dijet analysis with a smaller up-quark density at lower values x_γ (cf. also Fig. 14 in [3]). Here one must keep in mind that the full dijet analysis has been performed at larger values of $E_T \geq 20$ GeV (or Q) than the charm dijet analysis, where $E_T \geq 5$ GeV (see also Fig. 15 in [3] for the evolution of the CJK charm density with Q^2).
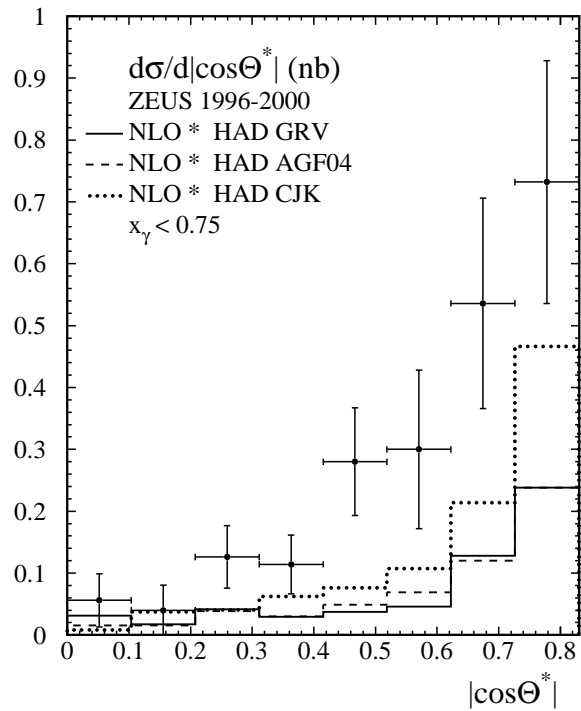
FIG. 11: Differential cross section $d\sigma/d|\cos\Theta^*|$ with the constraint $x_\gamma < 0.75$ for GRV, AFG04 and CJK photon PDFs compared to data of [10].

VI. CONCLUSION

In summary, we have demonstrated that the contribution of charm quarks to photoproduced dijets at HERA is substantial with charm quarks (or mesons) accounting for about one-third of all photoproduced dijets. This is in good agreement with the naive estimate of 2/5 from the sum of the squared quark charges coupling to the photon and offers the possibility to constrain the charm quark density in the photon.

To this end, we have computed the charm dijet photoproduction cross section at NLO of QCD in the zero-mass variable flavour number scheme, i.e. with active charm quarks in the proton and photon. This approach is justified by the fact that at large values of transverse energy the charm quark mass may safely be neglected, so that the contributions of collinear charm quark excitations may be resummed into parton densities in the photon and proton.

Our theoretical results were compared to recent measurements from the ZEUS experiment at HERA. The distributions in the photon and proton momentum fractions and the dijet scattering angle agreed well with the data, in particular for large momentum fractions of

16

the partons in the photon, where direct photon processes dominate. At low momentum fractions, the predictions were quite sensitive to the charm content in the photon.

We demonstrated that the experimental data favoured parameterizations, like the one by the CJK collaboration, with a substantial charm quark density. Since the total dijet cross section is overestimated by this parameterization, at least at low momentum fractions of the partons in the photon, it may, however, be necessary to compensate the higher charm-quark density with a smaller up-quark density. The logical next step would thus be to perform a global analysis of $F_2^\gamma(x)$ and dijet photoproduction data to better constrain the different flavours in the photon PDFs.

[1] H.-L. Lai et al., Phys. Rev. D82 (2010) 074024 and the references to earlier work therein.

[2] A. D. Martin, W. J. Stirling, R. S. Thorne and G. Watt, Eur. Phys. J. C63 (2009) 189 and the references to earlier work therein.

[3] F. Cornet, P. Jankowski and M. Krawczyk, Phys. Rev. D70 (2004) 093004.

[4] P. Aurenche, M. Fontannaz and J. Ph. Guillet, Eur. Phys. J. C44 (2005) 395.

[5] W. Slominski, H. Abramowicz and A. Levy, Eur. Phys. J. C45 (2006) 633.

[6] M. Glück, E. Reya and A. Vogt, Phys. Rev. D45 (1992) 3986, ibid. D46 (1992) 1973.

[7] P. Aurenche, J. Ph. Guillet and M. Fontannaz, Z. Phys. C64 (1994) 621.

[8] S. Chekanov et al., ZEUS Collaboration, Phys. Rev. D76 (2007) 072011.

[9] J. Breitweg et al, ZEUS Collaboration, Eur. Phys. J. C6 (1999) 67.

[10] S. Chekanov et al., ZEUS Collaboration, Phys. Lett. B565 (2003) 87.

[11] S. Chekanov et al., ZEUS Collaboration, Nucl. Phys. B729 (2005) 492.

[12] S. Frixione et al., Phys. Lett. B348 (1995) 633; S. Frixione et al., Nucl. Phys. B454 (1995) 3.

[13] M. Klasen and G. Kramer, Z. Phys. C72 (1996) 107; ibid. C76 (1997) 67; M. Klasen, T. Kleinwort and G. Kramer, Eur. Phys. J. direct C1 (1998) 1.

[14] M. Klasen, Rev. Mod. Phys. 74 (2002) 1221.

[15] J. Pumplin et al., JHEP 0207 (2002) 012.

[16] C. Amsler et al., Particle Data Group, Phys. Lett. B667 (2008) 1.

[17] S. Catani et al., Nucl. Phys. B406 (1993) 187, S. D. Ellis and D. E. Soper, Phys. Rev. D48 (1993) 3160.

[18] M. Klasen and G. Kramer, Phys. Lett. B366 (1996) 385; S. Frixione and G. Ridolfi, Nucl. Phys. B507 (1997) 315.

[19] L. Gladilin, hep-ex/9912064 (1999), unpublished.

[20] S. Chekanov et al, ZEUS Collaboration, Report DESY 03-015, February 2003, enlarged version of [10].

[21] M. Glück, E. Reya and I. Schienbein, Phys. Rev. D60 (1999) 054019 [Erratum-ibid. D62 (2000) 019902].